

## **General Disclaimer**

### **One or more of the Following Statements may affect this Document**

- This document has been reproduced from the best copy furnished by the organizational source. It is being released in the interest of making available as much information as possible.
- This document may contain data, which exceeds the sheet parameters. It was furnished in this condition by the organizational source and is the best copy available.
- This document may contain tone-on-tone or color graphs, charts and/or pictures, which have been reproduced in black and white.
- This document is paginated as submitted by the original source.
- Portions of this document are not fully legible due to the historical nature of some of the material. However, it is the best reproduction available from the original submission.



This report contains information prepared by Norman Cohen Professional Services under JPL sub-contract. Its content is not necessarily endorsed by the Jet Propulsion Laboratory, California Institute of Technology, or the National Aeronautics and Space Administration.

No reportable items of new technology have been identified.

## TABLE OF CONTENTS

	<u>PAGE</u>
<b>Abstract</b>	<b>1</b>
<b>Section 1</b> <b>Introduction</b>	<b>3</b>
<b>Section 2</b> <b>Model Premises and Assumptions</b>	<b>6</b>
2.1      Representation of the Solid Phase	6
2.2      Representation of the Gas Phase	9
2.3      Representation of Multimodal Propellants	10
2.4      Approach	10
<b>Section 3</b> <b>The Steady-State Model</b>	<b>12</b>
3.1      Solid Phase Equations	12
3.2      Gas Phase Equations	16
<b>Section 4</b> <b>The Time-Dependent Model: Calculation of the Response Function</b>	<b>18</b>
4.1      Solid Phase Equations	18
4.2      Gas Phase Equations	23
4.3      Solution for the Response Function	25
<b>Section 5</b> <b>Model Results</b>	<b>31</b>
5.1      The Steady-State Model	31
5.2      The Time-Dependent Model	35
<b>Section 6</b> <b>Conclusions and Recommendations</b>	<b>42</b>
<b>Section 7</b> <b>References</b>	<b>43</b>

## ABSTRACT

The objective of this program was to develop a computerized mathematical model of the combustion response function of composite solid propellants, with particular attention to the contributions of the solid phase heterogeneity. Such a model would be useful to design propellant formulations that would minimize the tendency to drive combustion instability in given applications. Although it is established that ammonium perchlorate particle size distribution has a significant effect upon this driving, previous models have treated all or portions of the combustion zone as homogeneous.

The one-dimensional model treats the solid phase as alternating layers of AP and binder, with an exothermic melt layer at the surface. Solution of the Fourier heat equation in the solid provides temperature and heat flux distributions with space and time. The problem is solved by conserving the heat flux at the surface from that produced by a suitable model of the gas phase. An approximation of the BDP flame model is utilized to represent the gas phase. By the use of several reasonable assumptions, it is found that a significant portion of the problem can be solved in closed form. A method is presented by which the model can be applied to tetramodal particle size distributions.

A computerized steady-state version of the model was completed, which served to validate the various approximations and lay a foundation for the combustion response modeling. The combustion response modeling was completed in a form which does not require an iterative solution, and some preliminary results were acquired.

It is concluded that the solid phase heterogeneity does per se influence the time lag and phase shift mechanisms responsible for combustion driving, and thereby the response function. Although the model was not fully evaluated by comparisons with experimental response function data, this conclusion is supported by the nature of the preliminary results. However, these results also indicate that the role of AP cannot be attributed to the solid phase alone -- at least insofar as the solid

phase is represented by this model. Potential deficiencies are identified, and areas of future work are recommended.

## SECTION 1

### INTRODUCTION

Experimental data have established that ammonium perchlorate (AP) particle size has a significant effect upon the pressure-coupled response function of composite solid propellants (1-14). Moreover, the effect cannot be attributed simply to changes in burning rate or formulation; the effect appears to involve the composite propellant heterogeneity as well (15). Classical theories of combustion driving (16) have assumed a homogeneous propellant, and are therefore inadequate to explain the combustion instability characteristics of composite propellants. The community has come to rely upon experimental measurement of the combustion response in T-burners, and work in recent years has been devoted largely to improving the method (17-19). Although experimental measurement serves several important purposes, interest in the theoretical work has revived because the acquisition and interpretation of full complements of data continue to be expensive and do not furnish a phenomenological mechanism for the guidance of propellant R&D.

Viewing the combustion zone as the region between the thermal wave penetration in the depth of the solid and the location of the flames in the gas, there are several ways in which the composite propellant heterogeneity can manifest itself. Two schools of thought have arisen: one which emphasizes the solid phase, treating the gas as a homogeneous source of propellant heating; and one which emphasizes the gas, continuing to treat the solid as a homogeneous medium.

The solid phase proponents may be represented by Lengelle & Williams (20), Kumar (21) and Cohen (13). Lengelle and Williams performed a one-dimensional analysis of a solid having sinusoidal thermal properties. Although the model was too idealized, it made the essential point that the heterogeneity augments the combustion response depending upon the periodicity of the thermal properties (and, therefore, particle size and spacing). Kumar introduced an exothermic surface melt layer, purportedly

representative of the AP surface, in an otherwise homogeneous solid. The most significant result of this model was a mechanism by which zero-exponent propellants could exhibit a positive combustion response and pressure effects.<sup>1</sup> Since Kumar did not treat in-depth heterogeneity, particle size effects appeared in the solid only through the effect of burn rate on melt layer thickness.<sup>2</sup> Cohen postulated two characteristic parameters for the solid phase, each dependent upon particle size. One was a measure of frequency response, the other of thermal response. He assumed that all response function curves could be determined by the pressure exponent plus these two parameters, and used experimental data for a standard propellant as calibration. The essential result is that decreasing particle size increases the peak response and shifts the peak to higher frequency. He further assumed that multimodel propellants could be treated by linear superposition of the constituent results, and predicted multi-peaked response functions. Although the method is not founded upon a formal analysis, it is being used to guide propellant tailoring (15, 22). Extensive applications have revealed some qualitative and quantitative deficiencies, for example a tendency to over-emphasize the effect of fine sizes (22).

The gas phase proponents may be represented by Hamann (23), Beckstead (24), and Glick and Condon (25). All utilize some form of the "BDP" model of steady-state combustion (26) to represent the gas phase details, and none consider the solid to be heterogeneous. Hamann performed a perturbation analysis upon the entire BDP model, but did not report any results. Beckstead used the BDP model to calculate values for the parameters which are called for by the homogeneous theory of Denison & Baum (27). This approach of combining unrelated models is

---

<sup>1</sup> The classical theories produce a response function proportional to pressure exponent, yet it is well known that plateau (zero exponent) and mesa (negative exponent) propellants have exhibited combustion instability. The AP melt may be analogous to the foam zone of such propellants.

<sup>2</sup> An effect of burn rate on melt layer thickness would also appear in double-base propellants, so cannot be a sole basis for the role of AP particle size in composite propellants. Furthermore, AP size effects persist at constant burning rate when catalysts are used or solids loading or distribution are varied.



open to question (15), and a review of the technique reveals several deficiencies.<sup>3</sup> Glick & Condon employed a similar approach, but used a modified BDP model (28) for polydisperse particle size distributions and the method of Zeldovich & Novozhilov (29) as an alternative to the theory of Denison & Baum. Comparison of results with experimental data was disappointing. Considerable improvement was noted, however, when the Cohen postulates were incorporated into the method to position the peak response and peak response frequency (25).

The following consensus appears to emerge from this background. First, there is a need to account for the melt layer and the in-depth solid phase heterogeneity of composite propellants. Second, there is a need to provide an analytical basis to test, confirm or modify the Cohen postulates. Third, the representation of the gas phase also should address the heterogeneity of composite propellants by embodying some form of the BDP model rather than the homogeneity of the classical theories. Accordingly, it was the objective of this program to develop an analytical model of the combustion response of composite solid propellants with particular attention to these contributions of the propellant heterogeneity.

---

3 For example, calculation of the "A" and "B" parameters of the homogeneous theory by this method reveals much too small a pressure effect to account for measured changes in the response function curve with pressure. As with Kumar, particle size effects appear only through changes in steady-state burning rate properties.

## SECTION 2

### MODEL PREMISES AND ASSUMPTIONS

#### 2.1 REPRESENTATION OF THE SOLID PHASE

The solid phase is represented by a "sideways sandwich", following the concept of Lengelle & Williams, as shown in Figure 1. This picture, really, does nothing more than state that the analysis is one-dimensional, so its dissimilarity to real propellants is of no greater concern than is the use of a one-dimensional treatment. Such a treatment assumes that the lateral processes are negligible in comparison to the normal processes. The solid is considered to be semi-infinite, having alternating layers of AP and binder. The thickness of the AP layers is nominally equal to the particle size, with exceptions to be noted later. The thickness of the binder layers is equal to the interstitial spacing as determined from the statistical geometry (26, 30). The surface AP layer contains a thin melt layer, which is justified experimentally (31-33), and follows the model of Kumar as a region of exothermic reactions in accordance with an Arrhenius law. The melt layer is "thin" in that the melting point of AP approximates the surface temperature during deflagration (32, 33). The analysis is linearized for small harmonic pressure perturbations, and is concerned with pressure-coupling only.

Although the model contains the convective heating term to represent the regression of the material at the mean rate  $\bar{r}$ , the geometry of the layers is taken to be fixed with the AP layer always at the surface. This assumption is similar to the statistically fixed geometry used in the BDP model. One consequence of this assumption is that the "pulsation" mechanism associated with moving layers is excluded. The pulsation mechanism is open to question in view of the aggregate macroscopic properties of the propellant, such that there is no coherence over the propellant surface for resonance, although Lengelle & Williams

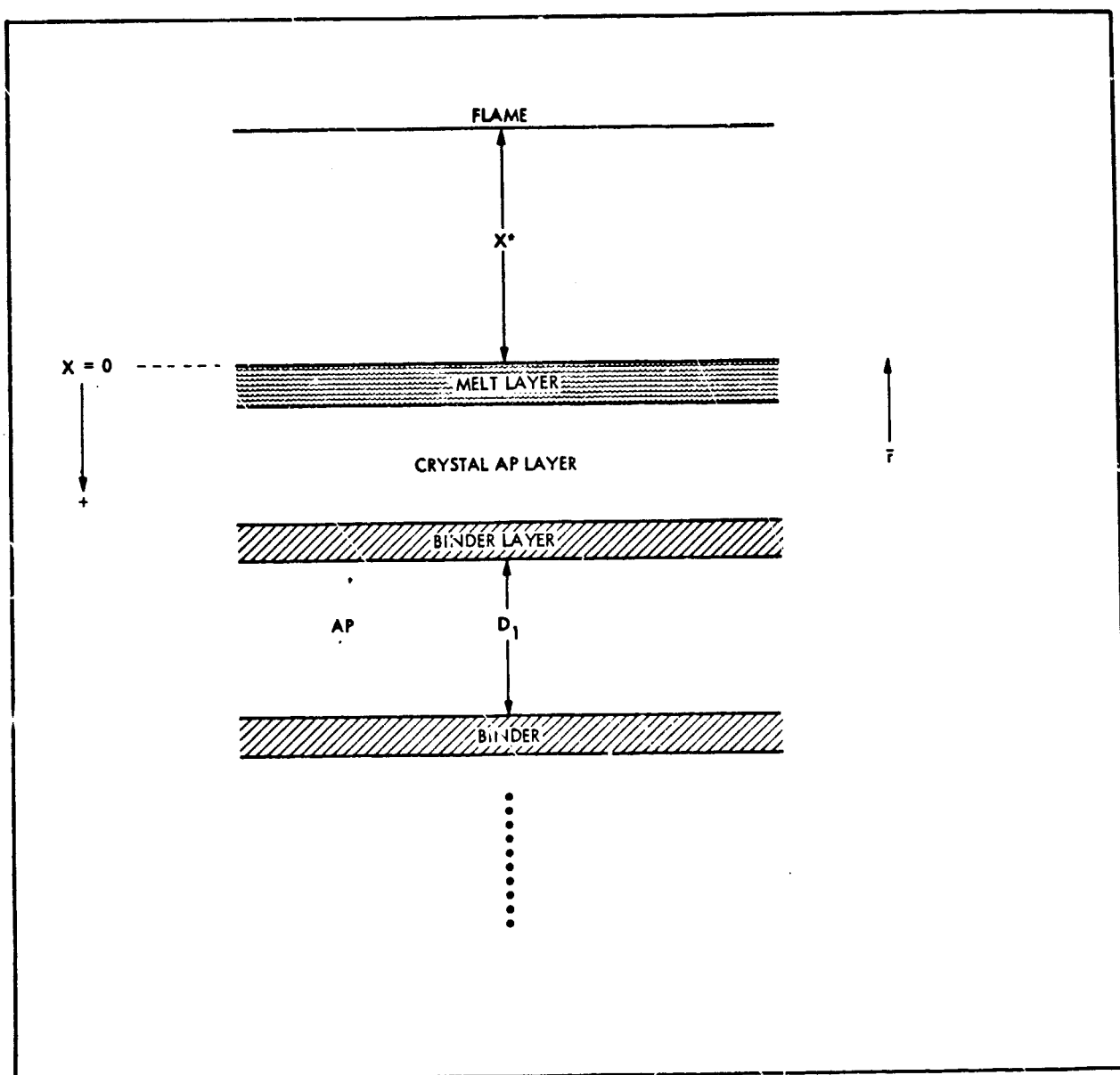


Figure 1. Physical Model Representation

offered an argument in its favor. In any event, the present physical model will not be conducive to such resonance because the thermal properties are not sinusoidal in space. Thus, the present model examines only the heterogeneity in relation to the thermal wave, which is a uniform property of the propellant and therefore considered more realistic at this point than pulsation. On the other hand, another consequence of this assumption is that in-depth heterogeneity will not be important in those cases where the particle size is larger than the thermal wave (generally, coarse particles and high burn rate). Whether or not this consequence is unduly restrictive remains to be seen, but the fact that catalyzed coarse propellants are more stable than fine propellants would seem to permit it. The statistically fixed geometry requires the surface AP layer (including the melt) to have a thickness  $\sqrt{2/3}$  of the particle size (26).

## 2.2 REPRESENTATION OF THE GAS PHASE

The function of the gas phase in the analytical scheme is to transform the oscillating pressure into an oscillating heat flux boundary condition at the surface of the AP melt. An approximate form of the BDP model has been selected to represent the gas phase, and the gas phase is assumed to be quasi-steady (viz, the gas phase responds instantly to changes in pressure). The approximation assumes a single flame above the propellant surface, where all gas phase reactions occur, as illustrated by Fig. 1.

Presuming that the condensed phase heterogeneity has the dominant effect upon the response function of composite propellants, it would not seem to matter what particular model were chosen to represent the gas so long as it provides a reasonable boundary condition. Thus, the Denison & Baum model could have been chosen to preserve some systematic order to the analytical development. This was not done for two reasons: First, it would have presumptuously ignored those developments addressing the gas phase heterogeneity in a BDP model framework. Second, the fact that the Denison & Baum model is heavily dependent upon fluctuations in flame temperature is coming to be viewed as a serious deficiency of that model. Variations in flame temperature are fourth order with respect to variations in pressure. On the other hand, variations in flame standoff, which are not addressed by Denison & Baum but which are a significant aspect of the BDP model (and a key to the particle size effects in the gas phase), are first order with respect to pressure variations.

The approach, then, is a perturbation of an approximate form of the BDP model with respect to flame standoff as well as flame temperature. Perturbation of the model itself is considered to be proper, whereas use of the model to calculate parameters for substitution into a different model is open to question. With the approximate model, the task is much simpler than that undertaken by Hamann.

### 2.3 REPRESENTATION OF MULTIMODAL PROPELLANTS

Multimodal propellants are represented by adjacent columns of layers, as shown by Figure 2. Each particle size tops a column, corrected by the factor  $\sqrt{2/3}$ . The remaining AP layers consist of the finest size in the distribution. This assumption is justified by the fact that the finest size will fill the smallest interstices between coarser particles, and will be valid so long as the thermal wave does not penetrate to a subsequent coarse sublayer. The assumption of limited thermal wave penetration will be valid for practical propellants because of the influence of the fine size in raising the burning rate. The binder layers are all of the same thickness, as computed by the method of Ref.(30). All of the columns are constrained to the same mean burning rate, which implies one effective flame height or characteristic size for the diffusion flame. However, the columns are allowed to have different response functions and the aggregate value for the propellant is a weighted average from the constituent columns.

### 2.4 APPROACH

The analysis is performed in two parts. First, the model is derived in its steady-state version. The steady-state version serves to calculate mean values required for the time-dependent model, verify that the boundary conditions will be reasonably accurate as measured by the ability to reproduce experimental (or formal BDP) results, establish the zero-frequency (no oscillation) limit, verify some of the model assumptions, and provide an initial check on the method of solving for the temperature profile in the solid. The steady-state model is one of the subroutines of the computerized response function model. Secondly, the time-dependent model for the combustion response function is derived. In calculating the response function, experimental values of mean burning rate are used as input in order to minimize the effects of uncertainties in the steady-state modeling.

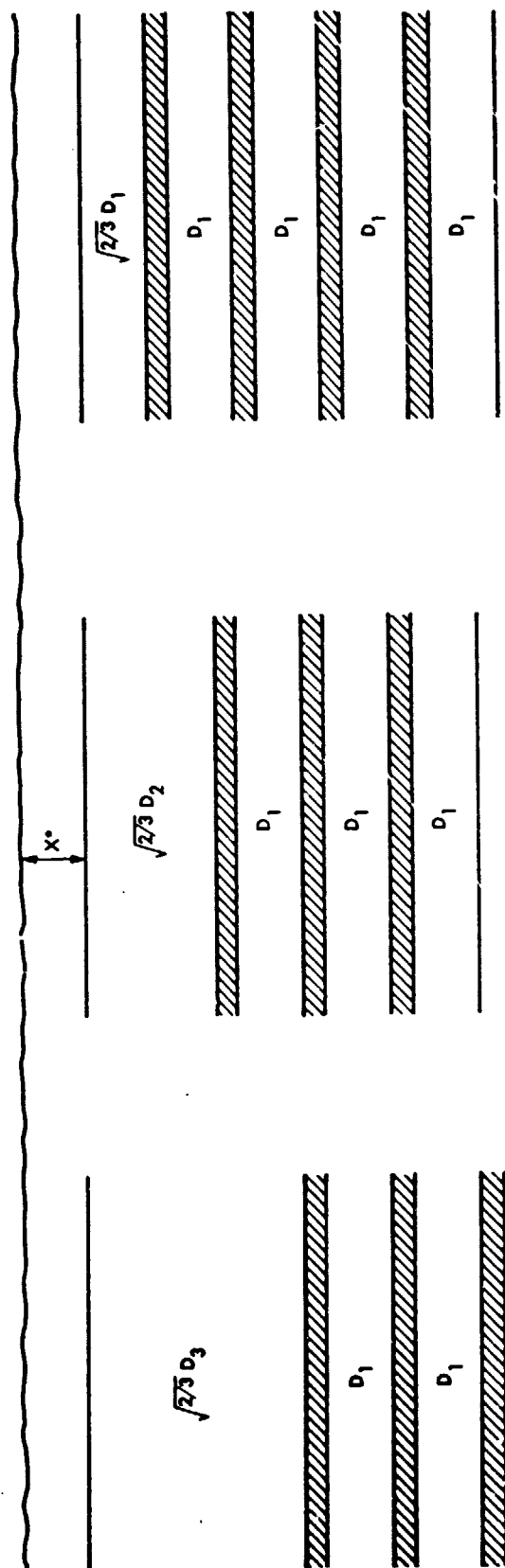


Figure 2. Layered Model of the Solid Phase for a Trimodal Propellant:  
 Sizes  $D_1$ ,  $D_2$ ,  $D_3$ . Shaded Layers are Binder. The Top of the  
 Surface AP Layer is a Thin Melt

# SECTION 3

## THE STEADY-STATE MODEL

### 3.1 SOLID PHASE EQUATIONS

The heat conduction equation in the melt layer is written as:

$$k_a \frac{d^2T}{dx^2} + \rho_a c_a r \frac{dT}{dx} = W_a \rho_a Q_a \exp(-E/RT) \quad (1)$$

where  $k$  = thermal conductivity

$\rho$  = density

$c$  = heat capacity

$W$  = weight fraction

$Q$  = heat of decomposition

subscript  $a$  = denotes AP

$A$  = kinetics prefactor

$E$  = activation energy

$R$  = gas constant

$r$  = burning rate

$T$  = temperature

$x$  = distance into the solid

The boundary conditions are:

$$x = 0, -k_a \frac{dT}{dx} = \rho_s c_s r (T_w - T_o) + W_a \rho_s r (Q_a + Q_m) \quad (2)$$

$$x = x_m, -k_a \frac{dT}{dx} = \rho_s c_s r (T_m - T_o) + W_a \rho_s r Q_m \quad (2)$$

where subscript  $w$  = denotes wall or surface

subscript  $s$  = denotes mean propellant

subscript  $m$  = denotes melt

subscript  $o$  = denotes the deep solid



Equation (1) may be written in dimensionless form as follows:

$$\frac{d^2\tau}{dy^2} + \frac{d\tau}{dy} = B \exp \left[ \frac{-E/RT_w}{\left( \frac{T_w - T_0}{T_w} \right) (\tau - 1) + 1} \right]$$

$$\text{where } \tau = (T - T_0)/(T_w - T_0)$$

$$y = \frac{r}{\kappa} x$$

$\kappa$  = thermal diffusivity of the medium,  $\kappa_a$  for Eq. (3)

$$B = A \frac{\kappa_a}{r^2} H_a \frac{C_s}{C_a}$$

$$H = \frac{WQ}{C_s (T_w - T_0)}$$

In the thin melt layer,  $\tau \sim 1$ , so Eq. (3) may be approximated as:

$$\frac{d^2\tau}{dy^2} + \frac{d\tau}{dy} = C \exp [-D(1-\tau)]$$

$$\text{where } C = B \exp (-E/RT_w)$$

$$D = \frac{E}{RT_w^2} (T_w - T_0)$$

The boundary conditions become:

$$\text{surface: } y = 0, \quad \frac{d\tau}{dy} = -Z_a (1 + H_a + H_m)$$

$$\text{melt/crystal: } y = y_m, \quad \frac{d\tau}{dy} = -Z_a (\tau_m + H_m)$$

$$\text{where } Z_a = \frac{\rho_s C_s}{\rho_a C_a}$$

Making the following transformation:

$$\xi = \tau + \frac{d\tau}{dy}$$

$$\eta = D(1-\tau)$$

Eq. (4) becomes:

$$(\xi - 1 - \eta/D) \frac{d\xi}{d\eta} = \frac{-C}{D} \exp(-\eta) \quad (8)$$

Recognizing  $\eta/D \ll 1$  where  $\tau \sim 1$ , and letting  $K = \frac{C}{D}$ , Eq. (8) becomes:

$$-\xi \frac{d\xi}{d\eta} + \frac{d\xi}{d\eta} = K \exp(-\eta) \quad (9)$$

Eqs. (5a & b) become:

$$\eta=0, \quad \xi = \xi_w = 1 - Z_a(1 + H_a + H_m) \quad (10a)$$

$$\eta=\eta_m, \quad \xi = \xi_m = \tau_m - Z_a(\tau_m + H_m) \quad (10b)$$

Eq. (9) may be integrated in closed form. Applying Eqs.(10) and some algebra yields an expression for burning rate in the following form:

$$K = \frac{\xi_w \left( \frac{\xi_w}{2} - 1 \right) - \xi_m \left( \frac{\xi_m}{2} - 1 \right)}{1 - \exp(-\eta_m)} \quad (11)$$

Making all substitutions, burning rate is expressed as a function of wall temperature and other constants as follows:

$$r^2 = \frac{\frac{2 \kappa_a A W_a Q_a}{C_a (T_w - T_0)} \frac{RT_w^2}{E(T_w - T_0)} \exp\left(-\frac{E}{RT_w}\right) \left[ 1 - \exp\left(-\frac{E}{RT_w} \frac{T_w - T_m}{T_w}\right) \right]}{\left\{ Z_a \left[ 1 + \frac{W_a (Q_a + Q_m)}{c_s (T_w - T_0)} \right] \right\}^2 - \left\{ \left( \frac{T_m - T_0}{T_w - T_0} \right) (1 - Z_a) - Z_a \frac{W_a Q_m}{c_s (T_w - T_0)} - 1 \right\}^2} \quad (12)$$

This relation is to be matched with a relation between burn rate and wall temperature from the gas phase model.

Analysis of the steady-state problem and, as will appear later, solution of the time-dependent problem, also require a description of the steady-state temperature profile in the solid. The temperature profile in the melt layer is determined from Eq. (9). Integration and application of Eq.(10a) yields:

$$\xi = 1 \pm \sqrt{1 + 2 [K \exp(-\eta) - C_M]} \quad (13)$$

$$\text{where } C_M = K - \frac{1}{2} [1 - Z_a(1 + H_a + H_m)]^2 + 1 - Z(1 + H_a + H_m)$$

The physics of the temperature decay requires the negative root. Substituting the definitions for  $\xi$  and  $\tau$  yields:

$$\frac{dn}{dy} = -n + D \sqrt{1 + 2 [K \exp(-n) - C_M]} \quad (14)$$

An order of magnitude analysis shows that the square root term will always be much larger than  $n$  in the melt layer. Thus, Eq. (14) reduces to the form:

$$\frac{dn}{\sqrt{a + b \exp(-n)}} = D dy \quad (15)$$

$$\text{where } a = 1 - 2C_M$$

$$b = 2K$$

This equation can be integrated in closed form for  $y(n)$ ; it is transcendental as  $n(y)$ .

$$y = \frac{1}{D\sqrt{a}} \ln \left[ \frac{1+z - \sqrt{z^2 + 2z}}{1+d - \sqrt{d^2 + 2d}} \right] \quad (16)$$

$$\text{where } d = 2a/b$$

$$z = d \exp(n)$$

The melt layer thickness may be calculated by evaluating Eq. (16) at  $n = n_m$ .

For all layers beneath the melt layer, the right-hand-side of Eq. (3) vanishes. The gradient condition at the top of each layer is similar to Eq. (5b), without the heat of fusion.

$$y = y_{\text{Top}}, \quad \frac{d\tau}{dy} = -Z \tau_{\text{Top}} \quad (17)$$

where  $Z = Z_a$  when entering an AP layer

$Z = Z_b$  when entering a binder layer

Thus the temperatures in each layer beneath the melt layer follow the recurring form:

$$\tau = \tau_{\text{Top}} - Z \tau_{\text{Top}} [1 - \exp(-\Delta y)] \quad (18)$$

where  $\Delta y$  = thickness of the particular layer, and uses the appropriate  $\kappa$ .

For a homogeneous propellant,  $Z=1$ , so Eq. (18) properly reduces to the result for a homogeneous propellant. Note also that the temperature and the gradient will properly tend to zero together, as  $y$  approaches infinity.

### 3.2 GAS PHASE EQUATIONS

If it is assumed that all reactions occur at the flame height, the heat conduction equation has the form of Eq. (1) with a zero right-hand-side. Taking the flame to be at  $x=0$  and the wall at the flame height ( $x=x^*$ ), the temperature distribution is:

$$T = T_f - (T_f - T_w) \frac{1 - \exp(-\zeta)}{1 - \exp(-\zeta^*)} \quad (19)$$

where  $\zeta = ux/\kappa_g$

$u$  = gas velocity normal to the surface

subscript  $g$  = denotes gas

subscript  $f$  = denotes flame

For convenience,  $\zeta$  is set equal to  $y$  by employing the continuity relation,  $\rho_g u = \rho_s r$ , and assuming that the ratio of heat capacity to thermal conductivity is equal for gas and solid<sup>4</sup>. Then the gradient at the wall may be written, from differentiation of Eq. (19), as:

$$y = y^* \frac{dT}{dy} = - (T_f - T_w) \frac{\exp(-y^*)}{1 - \exp(-y^*)} \quad (20)$$

where  $y^* = \frac{rx^*}{\kappa_s}$

---

4. This assumption is comparable to the general assumption that these properties are temperature-insensitive. The conductivity of propellant gases may be calculated, but is not well-known.

At the same time, the gradient at the wall must satisfy the energy requirements of the condensed phase:

$$-k_g \frac{dT}{dx} = \rho_s c_s r(T_w - T_o) + W_a \rho_s r(Q_a + Q_m) + W_b \rho_s Q_b \quad (21)$$

where subscript b = denotes binder

Eq. (21), when compared to Eq. (2a), states that the binder heat of decomposition is being positioned on the gas side of the wall. The binder does not appear at the surface in the model of Fig. 1, but does in reality exist over portions of the surface. The model surface is the AP melt. Therefore, in the framework of this model, the decomposing binder is external to the melt layer so may be represented by a heat absorption on the gas side. Eq. (21) may be re-written as:

$$y = y^*, -\frac{dT}{dy} = (T_w - T_o) + F \quad (22)$$

$$\text{where } F = (H_a + H_m + H_b)(T_w - T_o)$$

Equating Eq. (20) and Eq. (22) yields:

$$T_w = (T_f + F - T_o) \exp(-y^*) - (F - T_o) \quad (23)$$

which is the required matching relation in burn rate and wall temperature.

The remaining unknown,  $x^*$ , is determined by an approximate fit of the effective flame height from the BDP model:

$$x^* = C_F \frac{r D_1}{p} \quad (24)$$

where  $D_1$  = particle size

$p$  = pressure

$C_F = 24.6$  for  $r$  in cm/sec,  $p$  in atmospheres,  $D_1$  in microns and  $x^*$  in microns.

## SECTION 4

### THE TIME-DEPENDENT MODEL: CALCULATION OF THE RESPONSE FUNCTION

#### 4.1 SOLID PHASE EQUATIONS

Using dimensionless quantities as previously defined, the time-dependent heat conduction equation in the thin melt layer is written as:

$$\frac{\partial^2 \tau}{\partial y^2} + \frac{\partial \tau}{\partial y} - \frac{\kappa a}{r^2} \frac{\partial \tau}{\partial t} = C \exp[-D(1-\tau)] \quad (25)$$

Eq. (25) is the time-dependent form of Eq. (4). Denoting mean values as barred and perturbed values as primed, and employing Eq. (4) to describe the mean portion, Eq. (25) may be written as:

$$\frac{\partial^2 \tau'}{\partial y^2} + \frac{\partial \tau'}{\partial y} - \Omega \frac{\partial \tau'}{\partial (\omega t)} = C \exp(-\bar{\eta}) [\exp(D\tau') - 1] \quad (26)$$

where  $\omega$  = frequency of oscillations

$$\Omega = \frac{\kappa}{r^2} \omega$$

For harmonic perturbations,  $\tau' = \exp(i\omega t)$ , the time-dependent term of Eq. (26) may be re-written to provide an ordinary differential equation:

$$\frac{d^2 \tau'}{dy^2} + \frac{d\tau'}{dy} - i\Omega \tau' = C \exp(-\bar{\eta}) [\exp(D\tau') - 1] \quad (27)$$

If  $\tau'$  is of second order and  $\Omega$  sufficiently small, Eq. (27) may be approximated as:

$$\frac{d^2 \tau'}{dy^2} + \frac{d\tau'}{dy} = CD\tau' \exp(-\bar{\eta}) \quad (28)$$

The problem is linearized to small perturbations, and is therefore restricted to linear instability. Variations in burning rate are of the order of variations in pressure, but variations in surface temperature are second or third order with respect to variations in burning rate. Thus, for second order pressure perturbations,  $\tau'$  is at most of third order. The exponential in  $\bar{n}$  is approximately unity in the melt layer, and the product  $CD$  is of the order  $10^2$ . This would permit frequencies as high as 10KHz to satisfy the approximation for cases of interest. Since the quasi-steady assumption for the gas phase model will also restrict the frequencies to values less than 10KHz, use of Eq. (28) is satisfied by that assumption.

Applying the boundary conditions at the surface must recognize that the surface is fluctuating relative to the mean surface ( $y=0$ ) position. Since the fluctuating burning rate will also be of the form  $\exp(i\omega t)$  in the linearized problem, it follows that the surface position is given by:

$$y_S = -\frac{i}{\Omega} \frac{r'}{\bar{r}} \quad (29)$$

The boundary conditions are:

$$y = y_S, \quad \tau' = \tau'_W \quad (30a)$$

$$\frac{d\tau'}{dy} = Z_a \left( g'_W + \frac{r'}{\bar{r}} H_b \right) \quad (30b)$$

where  $g'_W$  = the gradient in  $\tau'$  at the surface, on  
the negative (gas) side of the boundary.

Eq. (30b) is derived by substituting Eq. (2a) into Eq. (21), and perturbing in the non-dimensional form. For small perturbations, the quantities at the actual surface may be related to the quantities at the mean surface as:

$$y = y_S, \quad \tau' = \tau'|_{y=0} - \frac{1}{\Omega} \frac{r'}{\bar{r}} \bar{g}|_{y=0} \quad (31a)$$

$$\frac{d\tau'}{dy} = g'|_{y=0} - \frac{1}{\Omega} \frac{r'}{\bar{r}} \frac{d\bar{g}}{dy} |_{y=0} \quad (31b)$$

where  $\bar{g}$  = the gradient in  $\bar{\tau}$

Eq. (28) is integrated numerically. The functions  $\exp(-\bar{\eta})$  and  $\bar{g}$  are available in terms of  $y$  from Eq. (16). The integration provides the mean surface values, which are then converted to the actual surface values by means of Eqs. (31). The actual surface values must satisfy Eqs. (30);  $g'_w$  is determined from the gas phase model, and  $\tau'_w$  is related to  $r'$  by perturbing Eq. (12). The perturbation of Eq. (12) yields:

$$\frac{r'}{\bar{r}} = V_5 \tau'_w \quad (32)$$

$$\text{where } V_5 = (1 + \frac{\theta}{2}) \chi + \frac{D}{2} \frac{1 - 2\chi(1 - \tau_m)}{\exp[D(1 - \tau_m)] - 1} - \frac{1}{Z_a(1 + H_a + H_m) - \tau_m(1 - Z_a) + Z_a H_m + 1}$$

$$\theta = E / (R \bar{T}_w)$$

$$\chi = (\bar{T}_w - T_0) / \bar{T}_w$$

Although the solution appears to require iteration, it will be shown subsequently that it does not (cf. Subsection 4.3).

For all layers beneath the melt layer, the right-hand-side of Eq. (27) vanishes so the time-derivative term cannot be neglected. Thus:

$$\frac{d^2 \tau'}{dy^2} + \frac{d\tau'}{dy} - i\Omega \tau' = 0 \quad (33)$$



The boundary conditions at each interface are generally:

$$y=y_{\text{Top}}, \tau'=\tau'_{\text{Top}} \quad (34a)$$

$$\frac{d\tau'}{dy} = \frac{Z_{a,b}}{Z_{b,a}} g'_{\text{Top}} \quad (34b)$$

where the first Z subscript is used when entering an AP layer and the second is used when entering a binder layer. Assuming that the product  $\rho c$  for the melt is equal to that for the solid AP, the ratio of Z does not appear for that first layer of solid AP which joins the melt. The  $g'_{\text{Top}}$  refers to that value of the perturbed gradient on the negative (upper) side of the boundary, which drives the behavior below. The  $\tau'_{\text{Top}}$ , however, is preserved on the positive side. Eq. (34b) is similar in form to Eq. (30b), but there is no phase change heat beneath the melt layer and the sublayers do not oscillate relative to the mean surface. Eq. (33) may be integrated to produce the following recurring formulas:

$$\tau'=\tau'_{\text{Top}} \exp(\lambda_1 \Delta y) - \frac{\lambda_1 \tau'_{\text{Top}} - \frac{Z_{a,b}}{Z_{b,a}} g'_{\text{Top}}}{\lambda_2 - \lambda_1} [\exp(\lambda_2 \Delta y) - \exp(\lambda_1 \Delta y)] \quad (35)$$

$$\frac{d\tau'}{dy} = \lambda_1 \tau'_{\text{Top}} \exp(\lambda_1 \Delta y) - \frac{\lambda_1 \tau'_{\text{Top}} - \frac{Z_{a,b}}{Z_{b,a}} g'_{\text{Top}}}{\lambda_2 - \lambda_1} [\lambda_2 \exp(\lambda_2 \Delta y) - \lambda_1 \exp(\lambda_1 \Delta y)] \quad (36)$$

$$\text{where } \lambda_1 = -\frac{1}{2} - \frac{1}{2} \sqrt{1+4i\Omega}$$

$$\lambda_2 = -\frac{1}{2} + \frac{1}{2} \sqrt{1+4i\Omega}$$

Each layer uses the appropriate ratio of Z, and the appropriate  $\kappa$  for  $\Delta y$ ,  $\lambda_1$  and  $\lambda_2$ .

Eqs. (35) and (36) properly reduce to the results for a homogeneous solid ( $Z=1$ , and the difference between  $g'$  and  $\lambda_1 \tau'$  vanishes throughout leaving only the first term on the right-hand-side). However, these equations retain the growing exponential term (in  $\lambda_2$ , of positive real part) for the layered solid because the formulation of the problem does not impose explicitly the boundary condition at infinity upon each layer. This condition is the requirement that  $\tau'$  and  $d\tau'/dy$  vanish together. For the homogeneous solid, this condition would immediately set the exponential in  $\lambda_2$  equal to zero. For the layered solid, it can only be said that a layer will eventually be reached where this condition may be approximated for all practical purposes. Since the effect of the heterogeneity on the perturbations also disappears when the perturbations disappear, this approximate condition may be expressed in the form of the homogeneous solid:

$$\tau' \rightarrow 0, \frac{d\tau'}{dy} \rightarrow \lambda_1 \tau' \quad (37)$$

In other words, there is a depth below which the propellant can be treated as homogeneous for purposes of the perturbation problem. Consider that this occurs below the  $N^{\text{th}}$  AP layer. Then Eq. (37) may be expressed as:

$$y=y_N, \tau' = \epsilon \quad (38a)$$

$$\frac{d\tau'}{dy} = \lambda_{1s} \epsilon \quad (38b)$$

where  $\epsilon$  = an extremely small number

$\lambda_{1s}$  = value of  $\lambda_1$  using  $\kappa_s$  for the homogeneous region.

Eq. (38b) represents the perturbed gradient at the top of the homogeneous region, on the positive (homogeneous) side of the boundary with the  $N^{\text{th}}$  AP layer. This may be converted to the perturbed gradient on the negative (AP) side of the

boundary through use of Eq. (34b), recognizing that  $Z=1$  in the homogeneous region. Thus, Eqs. (38) become:

$$y = y_N, \quad \tau_{\text{TopN}}^i = \epsilon \quad (39a)$$

$$g_{\text{TcpN}}^i = Z_a \lambda_{1s} \epsilon \quad (39b)$$

where subscript TopN = denotes the bottom of the  $N^{\text{th}}$  AP layer, which would be the "top" condition for the succeeding homogeneous region were the calculation to continue.

Thus, the problem of the solid phase is now properly closed. Eqs. (30) define the conditions at the "top", and Eqs. (39) define the conditions at the "bottom". The conditions at the bottom are now known, but the conditions at the top depend upon the gas phase. Additional discussion with respect to the solution for the solid phase is deferred to Subsection 4.3.

## 4.2 GAS PHASE EQUATIONS

The perturbed form of Eq. (24) is simply:

$$\frac{x^{\star i}}{\bar{x}^{\star}} = \frac{r^i}{\bar{r}} - \frac{p^i}{\bar{p}} \quad (40)$$

Since the analysis will take into account flame temperature perturbations, a relation between the flame temperature perturbations and the wall temperature perturbations is required. This is obtained by perturbation of Eq. (23). Using dimensionless quantities as previously defined, Eq. (40) for the flame standoff perturbations, and linearizing the exponential in perturbed quantities, there results:

$$\tau_f^i = \tau_w^i \exp(\bar{y}^*) - (1 + \tau_f) \bar{y}^* \exp(\bar{y}^*) \left[ \frac{p^i}{\bar{p}} - 2 \frac{r^i}{\bar{r}} \right] \quad (41)$$

$$\text{where } \tau_F = \frac{F}{\bar{T}_w - T_0}$$

The perturbed gradient on the gas side of the wall is derived from an energy balance. The energy being transmitted into the solid is the difference between the heat release in the gas and the energy required to raise the gas temperature to the flame temperature:

$$-k_g \frac{dT}{dx} = -\rho_s r Q_f - c_g (T_f - T_w) \quad (42)$$

where  $Q_f$  = heat release in the gas (negative for an exotherm).

Using the same relation between gas and solid thermal properties as led to Eq. (20), Eq. (42) may be written in dimensionless form as follows:

$$\bar{g}_w = H_f + (\bar{\tau}_f - 1) \quad (43)$$

where  $\bar{g}_w$  = gradient in  $\bar{\tau}$  at the wall on the negative (gas) side

$$H_f = \frac{Q_f}{\tau_g (\bar{T}_w - T_0)}$$

The perturbed dimensionless form of Eq. (42) is:

$$g'_w = \frac{r'}{\bar{r}} [H_f + (\bar{\tau}_f - 1)] + (\tau'_f - \tau'_w) \quad (44)$$

$H_f$  may be eliminated by combining the relations in Eqs. (43), (5a) and (21)<sup>5</sup>.

<sup>5</sup> For this purpose, Eq. (21) may be written as:  $d\bar{\tau}/dy = Z(\bar{g}_w + H_0)$ . This is the steady-state analog of Eq. (30b), and comes from substituting Eq. (2a) into Eq. (21) in dimensionless form.

Substitution into Eq. (44) yields:

$$g_w' = -\frac{r'}{\bar{r}} (1+\tau_F) + (\tau_f' - \tau_w') \quad (46)$$

Substitution of Eq. (41) into Eq. (46) yields, after combining terms:

$$g_w' = \frac{r'}{\bar{r}} (1+\tau_F)(2\bar{y}^* \exp(\bar{y}^*) - 1) + \tau_w' (\exp(\bar{y}^*) - 1) - \frac{p'}{\bar{p}} (1+\tau_F) \bar{y}^* \exp(\bar{y}^*) \quad (47)$$

Eq. (47) is the necessary matching relation for Eq. (30b). Thus, the formulation of the time-dependent problem is complete.

Eq. (45) also may be substituted into Eq. (43) to yield:

$$\bar{g}_w = -(1+\tau_F) \quad (48)$$

Eq. (48) is the dimensionless form of Eq. (22), so consistency is verified.

#### 4.3 SOLUTION FOR THE RESPONSE FUNCTION

By combination of Eqs. (30b), (31a), (31b), (32) and (47), it is possible to derive an explicit expression for the response function in terms of solid phase constants, gas phase constants and one key parameter characteristic of the solution for the solid phase. This key parameter is the ratio of the perturbed gradient to the perturbed temperature at the mean surface:

$$\left. \frac{g'}{\tau} \right|_{y=0} \equiv K_2 \quad (49)$$

The components of this ratio appear individually in Eqs. (31), and the ratio is defined here as  $K_2$ . In the classical homogeneous theory, this ratio is always  $\lambda_1$ . In this work, the ratio will depend upon the modeled heterogeneity and  $\lambda_2$  as well as on  $\lambda_1$ .

The expression for the response function is:

$$R = \frac{\Omega_a V_{6B}}{\Omega_a \left[ \frac{V_{6A}}{V_5} + 2V_{6B} - \frac{V_3}{Z_a} \right] + i \frac{C}{Z_a} - \frac{K_2}{Z_a} \left[ \frac{\Omega_a}{V_5} - i V_3 \right]} \quad (50)$$

Where  $R$  = response function

$$V_3 = Z_a(1+H_L+H_m) \text{ (see Eq. [5a])}$$

$$V_5 = \text{(see Eq. [32])}$$

$$C = \text{(see Eq. [4])}$$

$$V_{6A} = (\exp(\bar{y}^*)-1) \text{ (see Eq. [47])}, \text{ coefficient of } \tau_w'$$

$$V_{6B} = (1+\tau_F)\bar{y}^*\exp(\bar{y}^*) \text{ (see Eq. [47]), in coefficients of } p'/\bar{p} \text{ and } r'/\bar{r}.$$

If  $K_2$  depends upon  $g_w'$ , the problem will require an iterative solution. However, it turns out that  $K_2$  is an intrinsic property of the solid phase, independent of the surface boundary condition, just as is  $\lambda_1$  for the homogeneous solid. The reason is that the solid phase is described by linear homogeneous differential equations. All solutions of such equations of second order are of the form:

$$f = C_1 f_1(x) + C_2 f_2(x)$$

where  $f$  = denotes functions

$C_1$  = constant associated with surface boundary condition

$C_2$  = constant associated with deep solid condition

This form does not take into consideration the relative importance of the components of the BDP multiple flame structure and their differing dependencies upon the parameters of Eq. (24). However, it is a reasonable representation selected for mathematical convenience and with the perturbation analysis in mind.

After substitution of Eq. (24) into Eq. (23), Eqs. (12) and (23) are two equations for the unknowns  $r$  and  $T_w$ . These equations are solved by iteration. Once  $r$  and  $T_w$  are known, it is possible to calculate the melt layer thickness and the thermal profile in the solid.

The steady-state model is not intended to be used to calculate burning rates for multimodal propellants. That would require some definition of an effective particle size or flame height for use of Eq. (24). Rather, experimental values of burning rate are used to determine the wall temperature from the solid phase model, whence the effective flame height and particle size may be determined from the gas phase model. This is the general method for determining the mean values for use in the response function model. An option is provided to predict these values for unimodal propellants, and is used in this work only to validate aspects of the modeling. Those results are discussed in Section 5.

Note that the effects of particle size appear only as gas phase effects in the steady-state model. This conforms with a generally-accepted view of steady-state combustion (34). Although Eq. (12) (from the solid phase) may influence the magnitude of the particle size effect, particle size does not appear in that equation. The thermal profile in the solid does not enter into the calculation for mean burning rate. However, this does not preclude the importance of solid phase effects in determining the role of particle size in the time-dependent model for the response function.

The gradient is:

$$g = C_1 f_1'(x) + C_2 f_2'(x)$$

It is required that  $g/f$  go to  $\lambda_1$  in the deep solid. This provides a relation for  $C_2$ :

$$C_2 = C_1 \frac{f_1'(x) - \lambda_1 f_1(x)}{\lambda_1 f_2(x) - f_2'(x)}$$

Substituting this expression for  $C_2$  into the ratio  $g/f$ , it is verified that  $C_1$  cancels out. Of course,  $g/f$  will vary from case to case and will vary with  $x$  for a given case; the important point is that it does not depend upon  $C_1$ . This property was observed numerically in the course of computer program development, which was based initially upon an iterative scheme. Accordingly, it suffices to go through Eqs. (35) and (36) in the layers, beginning with Eqs. (39)<sup>6</sup>, and then solve numerically through the melt layer, just one time for  $K_2$ <sup>7</sup>. Knowing  $K_2$ , Eq. (50) for  $R$  is solved by complex arithmetic<sup>8</sup>.

It is of interest to examine the form of Eq. (50) in comparison to the form obtained from the homogeneous theory (Ref. 16). The latter can be written as:

$$R = \frac{\Omega n A B}{\Omega [A B - (1 + A)] + i A - \lambda_1 [\Omega - i A]} \quad (51)$$

where  $n$  = pressure exponent

$A$  = a solid phase parameter, not to be confused with  $A$  as defined in Eq. (1)

$B$  = a gas phase parameter, not to be confused with  $B$  as defined in Eq. (3)

$\lambda_1$  = as defined in Eqs. (35, 36); it is of opposite sign in Ref. (16).

6. Subroutine LAYRSP of the computer program

7. Subroutine MLTLRP of the computer program.

8. Subroutine GLIFP of the computer program.



It is noted that Eqs. (50) and (51) are identical in form and, to some extent, they are similar in substance. The parameter  $V_{6B}$  combines condensed phase and gas phase terms, as does  $(nAB)$  of Eq. (51). The parameters  $C$  and  $V_3$ , although different, are condensed phase terms as is  $A$  of Eq. (51). The parameter  $V_{6A}$  is a gas phase term, as is  $B$  of Eq. (51). The parameter  $V_5$  is related to  $C$ , and therefore, a part of the analogy to  $A$ ; but important differences from  $A$  derive from the finite melt layer. The parameter  $K_2$  is the heterogeneous analog of  $\lambda_1$ . The parameter  $Z_a$  is purely a consequence of the heterogeneity, so there would be no analog for it in Eq. (51). The identity in form, and the similarity in substance, suggests that the heterogeneity as described by this model will not produce radical changes in the qualitative behavior of the response function.

The zero-frequency limit of Eq. (51) is the pressure-exponent,  $n$ . Pressure exponent does not appear explicitly as such in the steady-state model described herein. Nevertheless, it is of interest to examine the zero-frequency limit of Eq. (50). It is readily apparent that a non-zero response function at zero frequency requires that the following relationship be satisfied:

$$\lim_{\Omega_a \rightarrow 0} K_2 = -\frac{C}{V_3} \quad (52)$$

The satisfaction of Eq. (52) is verified by combining Eqs. (31), (32), (5a), the derivative of Eq. (15) applied at  $y=0$ , and a perturbation of Eq. (2a). In general,  $K_2$  must be solved numerically, but at zero frequency it is possible to derive an expression which reduces to  $-C/V_3$ . Since Eq. (52) is satisfied, the indeterminate form of Eq. (50) that results may be evaluated to yield the non-zero response function:

$$\lim_{\Omega_a \rightarrow 0} R = \frac{V_{6B}}{2V_{6B} + \frac{1}{V_5} (1+V_{6A})} \quad (53)$$

Eq. (53) may be thought of as an "effective" pressure exponent, extracting an implicit property of the model. Note that it depends upon condensed phase terms as well as gas phase terms. Numerically, it is found to be consistent with pressure-dependence as calculated from results of the steady-state model.

## SECTION 5

### MODEL RESULTS

#### 5.1 THE STEADY-STATE MODEL

Results of the steady-state model have been obtained in order to evaluate some of the important model premises. The essential results are tabulated in Table I.

Table I presents various results, compared with data and with BDP model results, for A-13 propellant used as a standard case. The first set of results compares burning rate as a function of pressure. The model results compare very well with the data. It should be emphasized, however, that these results should not be construed to imply that this model is "better than" the BDP model. The second set of results compares surface temperature. Experimental values of surface temperature are reportedly in the neighborhood of 850°K (26). It is observed that this model produces higher surface temperatures than the BDP model, and a somewhat greater sensitivity to pressure. However, the results are reasonable. The results also confirm the assumption that variations in surface temperature are second order (or smaller) with respect to variations in burning rate. The third set of results compare flame standoff distance. This model uses one flame. The BDP results are for the primary flame (sum of diffusion and reaction heights), and the values to the right of the slash are for the AP monopropellant flame when that flame moves closer to the surface than the primary flame. When that happens, the BDP model employs an energy partitioning which may be thought of as some single flame having an effective height between the two shown. On that basis, the flame heights from this model are roughly a factor of 3 greater than from the BDP model but the qualitative behavior with pressure is the same. The value of  $C_F$  in Eq. (24) was adjusted to achieve good agreement with the burning rate data; values of other constants

TABLE I: COMPARISONS OF BURNING RATE AND OTHER  
QUANTITIES FOR A-13 PROPELLANT

<u>BURNING RATE</u>	<u>PRESSURE (PSIA)</u>	<u>DATA (cm/sec)</u>	<u>FROM EDP MDEL</u>	<u>FROM THIS MODEL</u>
	100	0.27	0.29	0.28
	300	0.41	0.39	0.47
	500	0.52	0.47	0.55
	700	0.62	0.53	0.65
	900	0.73	0.60	0.74
	1100	0.85	0.65	0.83
<u>WALL TEMPERATURE</u>				
	100	---	824°K	864
	300	---	836	900
	500	---	844	937
	700	---	851	973
	900	---	855	982
	1100	---	859	986
<u>FLAME HEIGHT</u>				
	100	---	25.6μ	82.9
	300	---	20.7	50.8
	500	---	19.9/18.3	35.7
	700	---	19.5/5.7	30.2
	900	---	19.4/3.1	25.8
	1100	---	19.3/3.1	23.6

are the same as used in the BDP model. It is concluded that, for purposes of the time-dependent analysis, the model conforms reasonably well with steady-state reality.

The ability to reproduce measured effects of AP particle size on burning rate was tested with a series of propellants analogous to A-13. These propellants were the subject of a low pressure  $L^*$  instability study performed by Ramohalli (35). The comparison of burning rates at 100 psia is as follows:

<u>PARTICLE SIZE(<math>\mu</math>)</u>	<u>DATA (cm/sec)</u>	<u>MODEL (cm/sec)</u>
40	0.41	0.38
90	0.27	0.28
200	0.23	0.19
360	0.19	0.13

Again, the agreement is reasonable.

There are two other aspects of the steady-state model results which merit discussion: the melt layer and the heterogeneity in relation to the thermal wave.

The melt layer thickness is computed to be of the order of microns or less, which is consistent with experimental observation and the thin melt layer assumption. Its dependence upon heating rate involves a tradeoff between surface temperature and the steepness of the thermal gradient. Theoretically, it will disappear at such low burning rate that the surface temperature does not reach the AP melting point, and also will approach zero at very high burning rate where the gradient is very steep. Although the layer is thin, it was considered improper to neglect it for mathematical convenience because the characteristic time of its dimension corresponds to high frequencies of interest.

For particle sizes in excess of  $40\mu$ , the thermal wave will not penetrate the first AP layer under conditions of interest. The implication is that, ex-

cept for the melt layer, the solid can be considered homogeneous in determining its role. However, this is not true for the fine sizes which are generally utilized in practical propellants. An estimate for a  $2\mu$  AP propellant reveals that, at 1000 psi, the temperature does not fall to within 10% of the bulk temperature until about 5 pairs of AP-binder layers are traversed. Further, if the  $2\mu$  AP is a component of a multimodal propellant, the burn rate will be lower such that the thermal wave will penetrate more layers of the column consisting of the  $2\mu$  AP. As a result, it appears that the role of solid phase heterogeneity will be limited to melt layer heterogeneity in the intermediate-coarse size regime, but that in-depth heterogeneity can be important in the fine size regime. This distinction is one consequence of the present fixed-geometry model; were the layers permitted to move to evoke the pulsation mechanism, then the in-depth heterogeneity would always be important. The distinction was considered significant in view of the experimental importance of fine AP (15).

## 5.2 THE TIME-DEPENDENT MODEL

The effects of the solid phase heterogeneities are most likely to appear at combinations of fine AP and low burning rate. Therefore, a test case consisting of a  $2\mu$  AP propellant at a burning rate of 0.47 cm/sec was selected for evaluation. Except for the particle size, this test case would correspond to A-13 propellant at 300 psi. Results are shown in Fig. 3. The solid line is for the heterogeneous propellant. The long-dash line is for AP and binder thermal properties equal to mean propellant thermal properties; therefore, it is for melt layer heterogeneity only, the propellant below the melt layer being homogeneous<sup>9</sup>. The short-dash line is for a completely homogeneous solid; i.e., the distributed heat release in the finite melt layer is now concentrated at the surface only and the entire region beneath the surface is homogeneous<sup>10</sup>. It is observed that the effects of the heterogeneities are small.

Figure 4 compares results for a  $90\mu$  AP propellant, which is A-13 propellant, with the Figure 3 results. Thus, the effect of particle size at a constant burning rate is shown. In the framework of this model, a constant burning rate implies a constant wall temperature and constant dimensionless flame properties; thus, any difference is due to solid phase heterogeneities. An effect of the heterogeneity does appear, but again, it is small. It is noted that the results for A-13 are virtually identical to the homogeneous solution displayed in Fig. 3. In the case of A-13, the thermal wave does not penetrate the surface AP layer and the melt layer thickness is about 1% of the particle size; thus, the solid is homogeneous for all practical purposes. In the case of the  $2\mu$  propellant, the thermal wave penetrates 15 AP layers and the melt layer thickness is about 1/3 of the particle size; thus, the solid is heterogeneous, but the effect of the

9-  $k_a = k_b = k_s$ ;  $\rho_a = \rho_b = \rho_s$ ;  $c_a = c_b = c_s$ ;  $Z=1$ .

10-  $V_3 = C = Z = 1$ ;  $K_2 = \lambda_1$ ;  $V_5 = \theta \cdot \chi$ . This would correspond to the Denison and Baum model except for differences in the modeling of the gas phase, and differences in the values of combustion constants due to the use of this model (including the finite melt layer) to reproduce steady-state burning rates.

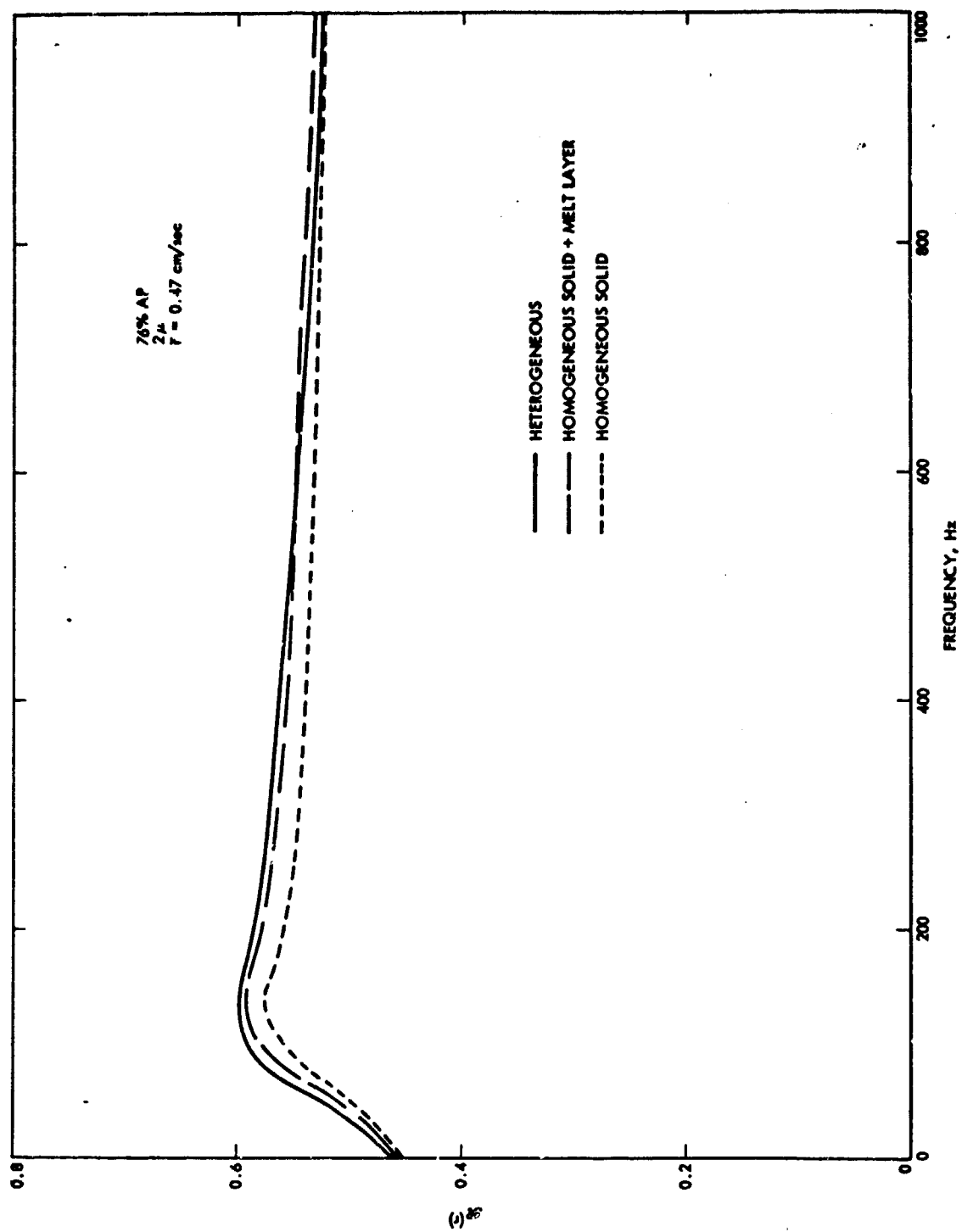


Figure 3. Response Function Calculations for a 2  $\mu$ AP Analog of A-13 Propellant



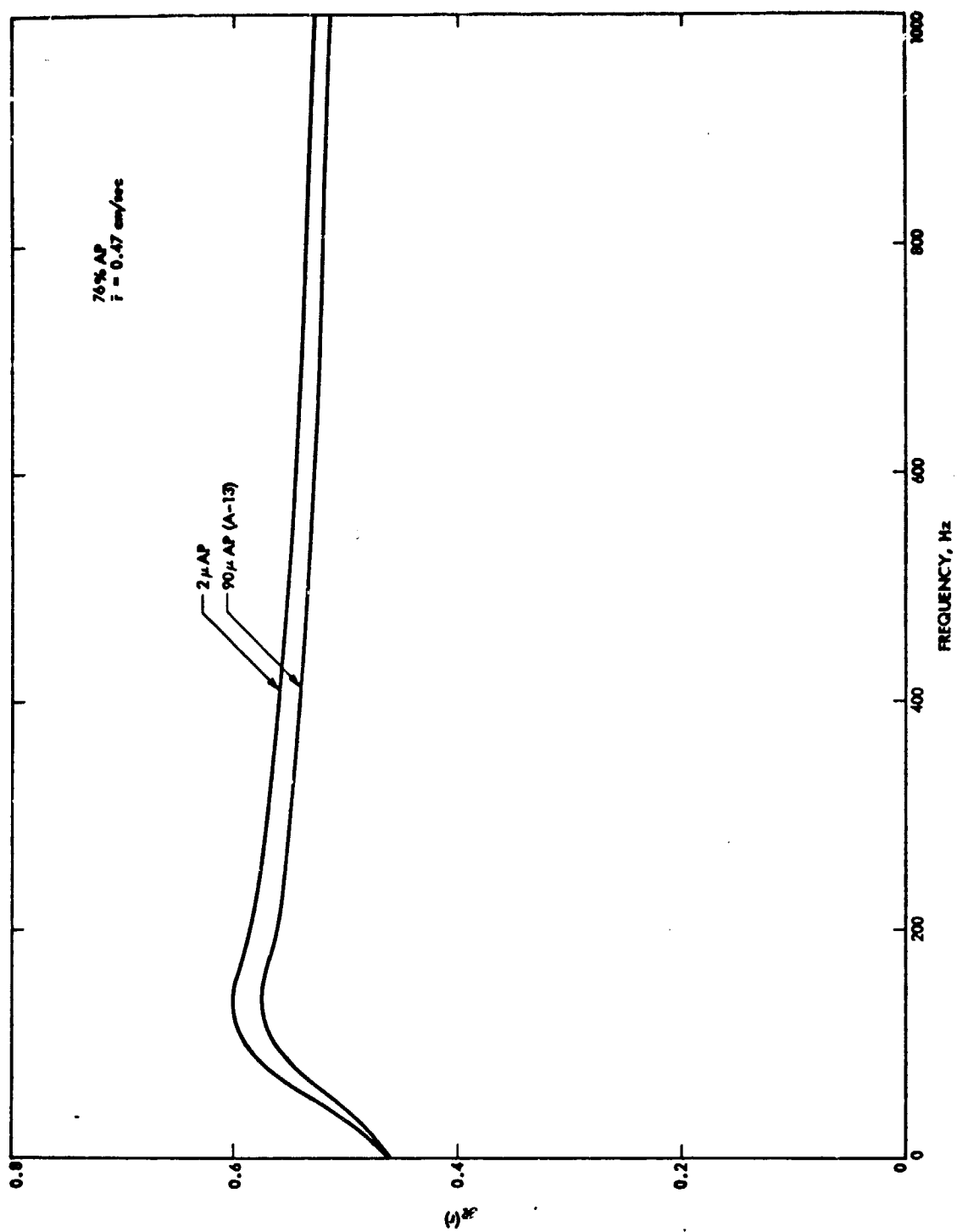


Figure 4. Effect of AP Particle Size at Constant Burning Rate for A-13 Type Propellant

heterogeneity appears to be small. Significantly, the effect is small with respect to peak response frequency as well as magnitude. Thus, it can be concluded that the expected effects of the heterogeneity are not being represented by this model.

The theoretical results for the A-13 propellant, moreover, do not agree with experimental data. The A-13 is a JANNAF standard propellant, and has been well-characterized in T-burner testing (Ref. 36). The experimental peak response is about 4 and occurs at roughly 300 Hz. Thereafter, the response declines to a value of approximately 1.5 at 1000 Hz. These theoretical results show a peak response of 0.58 at 125 Hz, and a value of 0.51 at 1000 Hz. Therefore, the theory shows a relatively slight peak and at too low a frequency. Such theoretical results are a consequence of the combustion parameters, analogous to the "A" and "B" (or " $\alpha$ ") parameters of the Denison and Baum model. Presumably, the agreement with data could be improved by selection of a different set of parameters. However, a ground rule of this study was that the parameters would be predetermined by considerations of a credible steady-state model. Given that model, it is inappropriate to change the constants arbitrarily. According to Ref. (27), a relatively large value of the "B" (or " $\alpha$ ") parameter will constrain the time-dependent model to the prediction of small peaks, and a relatively small value of the "A" parameter will produce low peak response frequencies. By analogy, that is the situation here. Since it would be inappropriate to juggle parameters, it must be concluded that there is a mechanistic deficiency in the time-dependent model.

Figure 5 presents theoretical results showing the effect of burning rate for a constant particle size. The 2 $\mu$  AP propellant was selected for this illustration. The higher burning rate is representative of this propellant; the lower burning rate may be thought of as a suppression for purposes of Figures 3 and 4. The effect on peak response frequency demonstrates further that the modeled heterogeneities are of little consequence. It is observed that the peak response frequency varies nearly with the square of the burning rate, which is the result

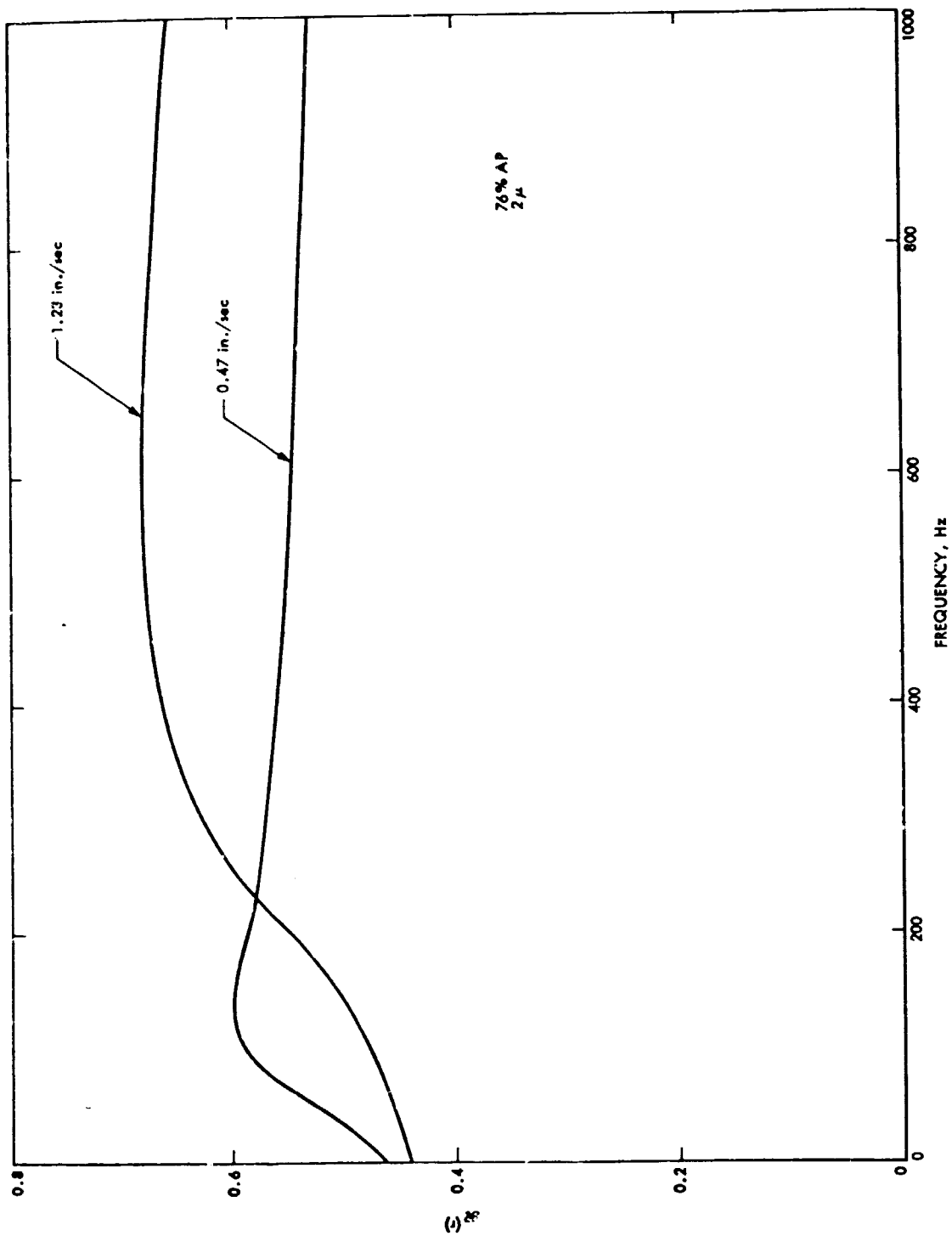


Figure 5. Effect of Burning Rate at Constant AP Particle Size for the 2  $\mu$  Analog of A-13 Propellant

for homogeneous propellants. On the other hand, the Fig. 3 and 4 results show that the effect of the heterogeneity on peak response frequency is about 10%. According to the Cohen postulates for the effect of heterogeneity, the peak response frequency in Fig. 5 should vary with the first power of burning rate, and in Fig. 4 it should vary inversely with particle size. These effects are not being produced by this model.

Figure 6 compares theoretical results with experimental data for a bimodal propellant. Although the shape of the theoretical curve is reasonable, the peak response magnitude and frequency are again underpredicted. Also, the zero frequency limit is overpredicted, reflecting a deviation from the measured steady-state pressure exponent. It appears that further work is necessary in order to implement a proper mechanism for the combustion response.

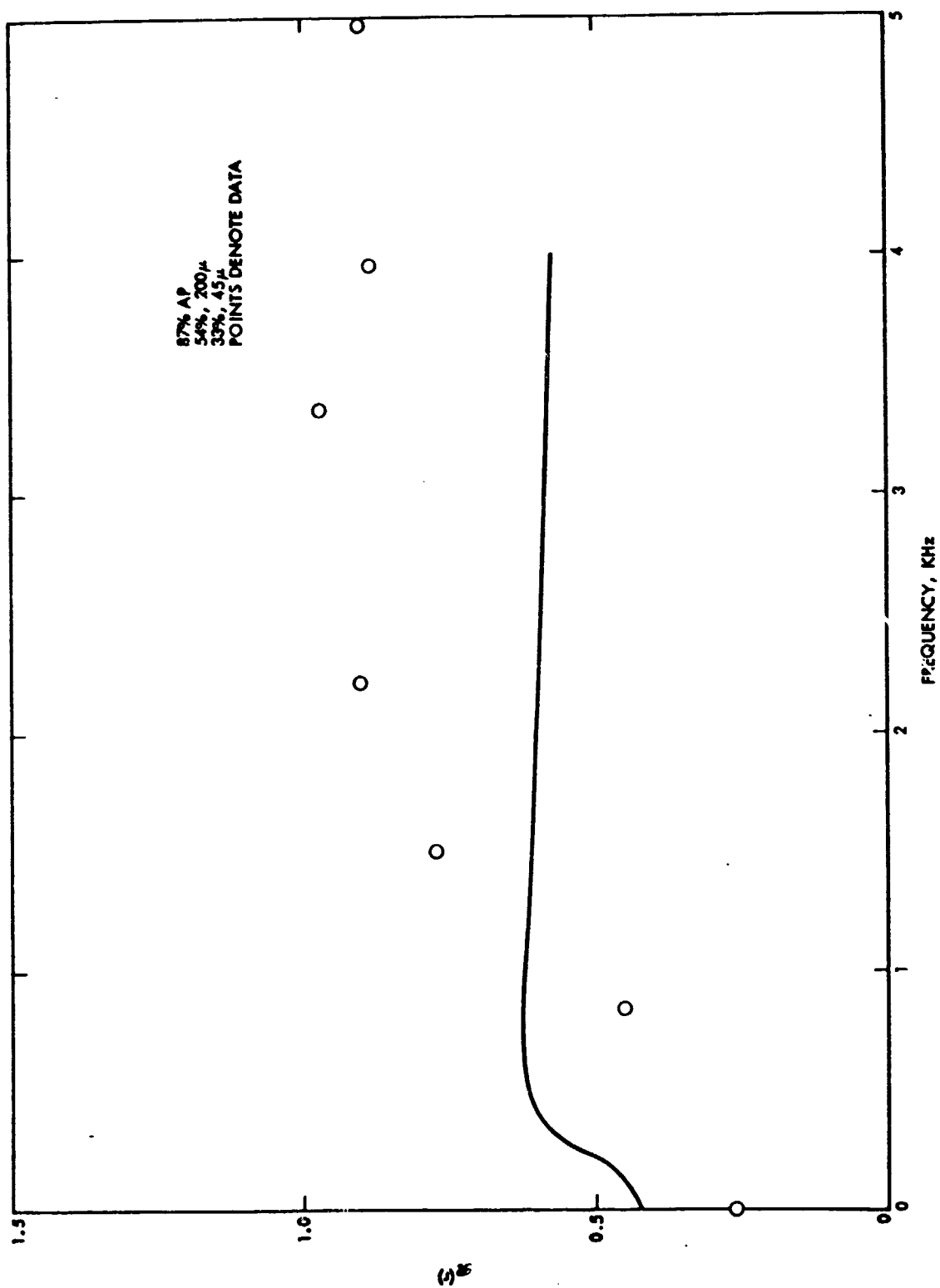


Figure 6. Comparison of Theory and Experiment for SP-540 Propellant at 500 psi

## CONCLUSIONS AND RECOMMENDATIONS

An analytical model has been developed which incorporates mechanisms of solid-phase and gas phase heterogeneities into the calculation of steady-state and linear time-dependent combustion properties of composite solid propellants. Although the model satisfactorily describes the steady-state combustion properties, it is deficient in describing the time-dependent combustion response characteristics in several respects. Use of a consistent set of combustion constants produces peak response magnitudes and frequencies which are too low in comparison to experimental data, and which are not significantly affected by the AP particle size per se. Although an effect of the solid phase heterogeneities is predicted by this model, the effect is so small quantitatively as can be neglected in future work. Therefore, the role of AP cannot be attributed to the solid phase alone unless some other mechanism is incorporated into the theory. It is recommended that the concept of moving layers be re-examined, including justification for the coherence of such a mechanism. It is further recommended that the perturbed BDP model be examined to represent the heterogeneity of the gas phase. It is desired not only to achieve the effects of the heterogeneity, but also to justify a set of values of the combustion constants that will properly position the response function curve. It appears necessary to modify both the solid phase and gas phase models in order to achieve those purposes in a consistent manner.

## SECTION 7

### REFERENCES

1. Green, L.G., "Effects of Oxidizer Concentration and Particle Size on Resonance Burning of Composite Solid Propellants", Jet Prop. 28, 159-164 (Mar., 1958).
2. Strand, L.D., "Low Pressure  $L^*$  Instability and Extinction", 3rd ICRPG Combustion Conference (CPIA Publication 138, Vol. I, Feb., 1967) pp. 195-207.
3. "Experimental Studies on the Oscillatory Combustion of Solid Propellants", Report NWC-TP-4393, U.S. Naval Weapons Center, China Lake, CA (Mar., 1969).
4. Beckstead, M.W., Boggs, T.L. and Madden, O.H., "The Effect of Oxidizer Particle Size and Binder Type on Nonacoustic Instability", AIAA Paper 69-175 (1969).
5. Boggs, T.L. and Beckstead, M.W., "Failure of Existing Theories to Correlate Experimental Nonacoustic Combustion Instability Data", J. AIAA 8, 626-631 (Apr., 1970).
6. Crump, J.E., "Combustion Instability in a Series of AP-HTPB Smokeless Propellants", 8th JANNAF Combustion Meeting (CPIA Publication 220, Vol. II, Dec. 1971) pp. 81-90.
7. Crump, J.E., "Combustion Instability Studies on Non-metallized AP-HTPB Propellants", 9th JANNAF Combustion Meeting (CPIA Publication 231, Vol. III, Dec., 1972) pp 123-134.
8. Wendelken, C.P., "Combustion Stability Characteristics of Solid Propellants", AFRPL-TR-73-C, Air Force Rocket Propulsion Laboratory, Edwards, CA. (Oct., 1973).
9. "Aluminum Behavior in Solid Propellant Combustion", AFRPL-TR-74-13, Lockheed Propulsion Company, Redlands, CA (May, 1974).
10. Micheli, P.L., "Stabilization of Smokeless Propellants with Additives", 11th JANNAF Combustion Meeting (CPIA Publication 261, Vol. III, Dec., 1974) pp 123-136.
11. Anderson, F.A. and Kumar, R.N., "Feasibility Study of Propellants and Igniters for Shuttle Solid Rocket Booster Separation Motors", Report 900-710, Jet Propulsion Laboratory, Pasadena, CA (June, 1975).
12. Cohen, N.S., et al., "Design of a Smokeless Solid Rocket Motor Emphasizing Combustion Stability", 12th JANNAF Combustion Meeting (CPIA Publication 273, Vol. II, Dec. 1975) pp. 205-220.
13. Horton, M.D. and Rice, D.W., "The Effects of Compositional Variables Upon Oscillatory Combustion of Solid Rocket Propellants", Combustion and Flame 8, 21-28 (Mar. 1964).

14. "Control of Solids Distribution in HTPB Propellants", Contract F04611-76-C-0006, Hercules Inc., Allegheny Ballistics Laboratory, Cumberland, MD (in progress).
15. Cohen, N.S., "Report of Workshop on Combustion Instability of Smokeless Propellants", Proceedings of 14th JANNAF Combustion Meeting (to be published).
16. Culick, F.E.C., "A Review of Calculations for Unsteady Burning of a Solid Propellant", J. AIAA 6, 2241-2254 (Dec., 1968).
17. "T-Burner Testing of Metallized Solid Propellants", AFRPL-TR-74-28, edited by F.E.C. Culick, Air Force Rocket Propulsion Laboratory, Edwards, CA (Oct., 1974).
18. "T-Burner Motor Verification Program Final Report", AFRPL-TR-74-71, Aerojet Solid Propulsion Company, Sacramento, CA (Jan., 1975).
19. Lovine, R.L. and Linfor, J.J., "Measurement of Propellant Response at High Frequency", 13th JANNAF Combustion Meeting (CPIA Publication 281, Vol. II, Dec. 1976) pp 95-112.
20. Williams, F.A. and Lengelle, G., "Simplified Model for Effect of Solid Heterogeneity on Oscillatory Combustion", Astronautica Acta 14, 97-118 (1968).
21. Kumar, R.N., "Some Considerations in the Combustion of AP/Composite Propellants", Report under Contract NAS 7-100, Guggenheim Jet Propulsion Center, California Institute of Technology, Pasadena, CA (Aug., 1972).
22. Glick, R.L., Private Communications, Thiokol Corp., Huntsville, AL (1977).
23. Hamann, R.J., "Three Solid Propellant Combination Models, A Comparison and Some Application to Non-Steady Cases", Memo. M-215, Delft University of Technology, Delft, Netherlands (Apr., 1974).
24. Condon, J.A., Osborn, J.R. and Glick, R.L., "Statistical Analysis of Polydisperse, Heterogeneous Propellant Combustion: Nonsteady-state", 13th JANNAF Combustion Meeting (CPIA Publication 281, Vol. II, Dec., 1976) pp 209-223.
25. Beckstead, M.W., "Combustion Calculations for Composite Solid Propellants", *ibid.*, 299-312.
26. Beckstead, M.W., Derr, R.L. and Price, C.F., "A Model of Solid Propellant Combustion Based on Multiple Flames", J. AIAA 8, 2200-2207 (Dec., 1970).
27. Denison, M.R. and Baum, E., "A Simplified Model of Unstable Burning in Solid Propellants", J. ARS 31, 1112-1122 (Aug., 1961).
28. Glick, R.L. and Condon, J.A., "Statistical Analysis of Polydisperse, Heterogeneous Propellant Combustion: Steady-State", 13th JANNAF Combustion Meeting (CPIA Publication 281, Vol. II, Dec., 1976) pp 313-345.
29. Novozhilov, B.V., "Nonstationary Combustion of Solid Rocket Fuels", Nauka, Moscow (1973).



30. Cohen, N.S., Price, C.F. and Strand, L.D., "Analytical Model of the Combustion of Multicomponent Solid Propellants", AIAA Paper 77-927, AIAA/SAE 13th Propulsion Conference (July, 1977).
31. Boggs, T.L., "The Decomposition, Pyrolysis and Deflagration of Ammonium Perchlorate", et seq., 7th JANNAF Combustion Conference (CPIA Publication 204, Vol. 1, 1971) pp 113-138.
32. Guirao, C. and Williams, F.A., "A Model for Ammonium Perchlorate Deflagration Between 20 and 100 atm", J. AIAA 9, 1345-1356 (July, 1971).
33. Beckstead, M.W. and Hightower, J.D., "Surface Temperature of Deflagrating Ammonium Perchlorate Crystals", J. AIAA 5, 1785-1790 (Oct., 1967).
34. Derr, R.L., "Review of Workshop on Steady State Combustion Modeling of Composite Solid Propellants", 7th JANNAF Combustion Meeting (CPIA Publication 204, Vol. I, 1971) pp 1-8.
35. Kumar, R.N. and McNamara, R.P., "Some Experiments Related to L-Star Instability in Rocket Motors", AIAA Paper 73-1300 (Nov., 1973).
36. "T-Burner Manual", CPIA Publication 191 (Nov., 1969).